

## Design of Tiny Versatile UHF RFID Tags of Fragment-Type Structure

Chenwei Yang<sup>1</sup>, Gang Wang<sup>1, 2, \*</sup>, and Dawei Ding<sup>1</sup>

**Abstract**—Small ultra high frequency (UHF) radio frequency identification (RFID) tags of fragment-type structure can be designed for broadband operation and for versatile impedance matching to different chips. The fragment-type tag structure can be optimized by using genetic algorithm. In our design, multi-objective evolutionary algorithm based on decomposition combined with enhanced genetic operators (MOEA/D-GO) is used for optimization searching. The multiple objectives are defined in terms of power transmission coefficients for operation in multiple RFID bands and for impedance matching to several prevailing RFID chips. For demonstration, a fragmented tiny square UHF tag of dimensions of 5.5 mm \* 5.5 mm is designed for multi-band operation over the 433 MHz, 869 MHz and 915 MHz RFID bands, and a fragmented round tiny RFID tag of radius of 4.5 mm is also designed for versatile connection to five prevailing RFID chips at 915 MHz. The tiny round versatile tag is tested by connecting two chips, the IMPIMJ Monza-4 chip (11 – 143j) and ALIEN Higgs-3 chip (27 – 195j), respectively. Effects of input impedance and adjunct fragments on versatility of the design are further discussed.

### 1. INTRODUCTION

In recent years, radio frequency identification (RFID) has found more and more applications in different fields, and various ultra high frequency (UHF) RFID tags have been developed. Nowadays, more stress of RFID is laid on application specific designs such as UHF RFID tag of antenna tolerance to variations in the platform [1, 2], RFID sensor tags [3–5], RFID-involved wearable technology [6] and green/renewable technology [7]. In these designs, traditional antenna structures with canonical geometry may become unpractical for RFID tags, and novel antenna structures are highly desired.

Fragmented geometry has been proposed for antenna design for years [8–12]. It is generally noted that fragment-type antennas may provide great convenience for impedance matching and broadband operation [13, 14]. Fragment-type antennas or structures should find application in UHF RFID tag design.

Recently, fragment-type antennas were considered in UHF RFID tag designs [15, 16]. In [15], RFID tags with fragment-type structures on area of 5 cm \* 5 cm were designed for EM4223 and Alien RFID chips operated at 869–960 MHz. In the design, approximately 1/4 of the tag antenna area was used for fragment metal cells. In [16, 17], impedance characteristics of fragment-type tag antennas were analyzed. It was reported that for different IC chips, different fragment-type antenna structures can be designed for impedance matching without much change to the design process. A universal design process for fragmented RFID tag design is quite reasonable.

In fact, advantages of fragment-type antennas can be carried forward in UHF RFID tag design in two more aspects. First, the broadband operation of fragment-type antenna will benefit the design of

---

*Received 3 April 2014, Accepted 13 July 2014, Scheduled 29 July 2014*

\* Corresponding author: Gang Wang (gwang01@ustc.edu.cn).

<sup>1</sup> Department of Electronic Engineering and Information Science, University of Science and Technology of China, Hefei 230027, China.

<sup>2</sup> Key Laboratory of Electromagnetic Space Information, Chinese Academy of Sciences, Hefei 230027, China.

UHF RFID tag suitable for multiple RFID bands, i.e., one tag may operate at different UHF RFID bands such as 433 MHz, 869 MHz and 915 MHz RFID bands. Second, flexible impedance matching performance of fragment-type antenna provides the possibility that different RFID chips may fit one tag structure. Therefore, versatile UHF RFID tag for multiple RFID operation bands and for different RFID chips can be desired if using fragment-type structure, which may benefit the design and production of RFID tags.

In practice, tiny UHF RFID tags may find more and more applications in small object identification such as medical test tube identification. The design of versatile and tiny UHF RFID tags is still a challenge. Although fragment-type structure allows designing RFID tags of different shapes according to different deployment requirements on small objects, it is still unknown whether or not fragment-type structures can be designed in a tiny UHF RFID tag which can operate on multiple UHF RFID bands or can connect to different prevailing RFID chips.

In this paper, we propose a scheme for designing tiny fragment-type UHF RFID tags that allow multi-band operation or versatile connection to different RFID chips. To this aim, multiple design objectives can be defined in terms of power transmission or reflection coefficient. Accordingly, design of a tiny versatile fragment-type tag forms a multi-objective problem. Several multi-objective evolutionary algorithms (MOEA) can be used to solve the multi-objective problem [18, 19]. In our design, multi-objective evolutionary algorithm based on decomposition with genetic operators (MOEA/D-GO) [20] is applied to solve the multi-objective problem for versatile fragmented UHF RFID tag design.

The paper is organized as follows. In Section 2, multi-objective problem of tag design for multi-band operation and versatile connection to different prevailing RFID chips are defined, and scheme for MOEA/D-GO fragmented tag design is introduced. In Section 3, we report the design of a fragmented tiny square UHF tag operating at the 433 MHz, 869 MHz and 915 MHz RFID bands, and the design of a fragmented round tiny RFID tag versatile for five prevailing RFID chips at 915 MHz. The round tiny tag is tested for verification by connecting to a commercial IMPINJ Monza-4 chip and an ALIEN Higgs-3 chip, respectively. In Section 4, effects of RFID chip impedance and adjunct fragment cells of the designed tag on tag performance are further analyzed. Both simulation and experiment results indicate that RFID tag with fragmented structure provide flexibility for different RFID chips.

## 2. MOEA-BASED FRAGMENTED TAG DESIGN

### 2.1. Description of Fragmented Tag Geometry

As shown in Fig. 1, fragment-type RFID tag structure can be described by gridding a designated tag area, assigning “1” and “0” to different cells, and filling cells marked “1” with metal cells. Generally, a design matrix can be defined according to the distribution of “1” and “0”, in a straightforward sequence or other specified sequence.

With the design matrix, different chromosomes can be readily defined for evolutionary algorithms. Design of a fragmented UHF RFID tag is to seek a proper design matrix to meet the objectives required by the tag performance.

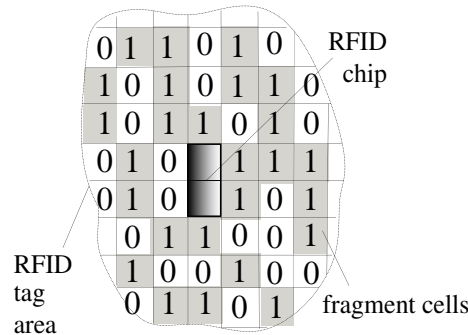


**Figure 1.** Definition of a fragmented RFID tag within a designated tag area.

## 2.2. Multiple Objectives for Multi-Band and Versatile Tags

In RFID tag design, efficiency of power transmitted from tag antenna to RFID chip is the major concern [21, 22]. Therefore, conjugate match between input impedance of an RFID chip and input impedance of a tag antenna is highly desired.

For fragmented RFID tag optimization, power wave reflection coefficient or power transmission coefficient, in terms of conjugate impedance match to UHF RFID chip, can be defined as objective for optimization. For RFID chip of input impedance  $Z_c$ , power wave reflection coefficient  $\Gamma_p$  [23] is defined as

$$\Gamma_p = \frac{Z_{ant} - Z_c^*}{Z_{ant} + Z_c}, \quad (1)$$

where  $Z_{ant}$  is the input impedance of fragmented tag antenna.

For different design requirements, different objectives can be defined. In terms of the conventional  $-10$  dB reflection loss requirement, two typical design scenarios are as follows:

1) For design of UHF RFID tag with multiple operation bands (e.g., there are  $m$  operation bands), we may define multiple objectives as

$$f_i(x) = \max(10 - \min_{\omega_i \in [\omega_{i1}, \omega_{i2}]} |\Gamma_p|, 0) \quad (i = 1, 2, \dots, m), \quad (2)$$

where  $[\omega_{i1}, \omega_{i2}]$  ( $i = 1, 2, \dots, m$ ) defines the  $i$ th operation band. It should be remarked that one objective may be defined if broadband operation covering the  $m$  bands can be obtained.

2) For design of UHF RFID tag with a versatile structure to connect different RFID chips (e.g., there are  $m$  chips to match), we may define multiple objectives as

$$f_i(x) = \max(10 - |\Gamma_{pi}|_{\omega_i \in [\omega_{i1}, \omega_{i2}]}, 0) \quad (i = 1, 2, \dots, m), \quad (3)$$

where  $[\omega_1, \omega_2]$  defines the operation band and  $\Gamma_{pi}$  represents the power wave reflection coefficient when connected to the  $i$ th chip, i.e.,

$$\Gamma_{pi} = \frac{Z_{ant} - Z_{ci}^*}{Z_{ant} + Z_{ci}} \quad (i = 1, 2, \dots, m), \quad (4)$$

In (4),  $Z_{ci}$  is the input impedance of the  $i$ th RFID chip.

To characterize tag read range as in [21], power transmission coefficient could be more convenient. In terms of  $\Gamma_p$ , power transmission coefficient can be calculated by

$$T_p = 1 - |\Gamma_p|^2, \quad (5)$$

thus the  $-10$  dB reflection loss indicates  $-0.46$  dB power transmission coefficient. The objectives in (2) and (3) can also be defined in terms of power transmission coefficients.

With the objectives defined above, the multi-objective problem for fragment-type RFID tag design is generally given as

$$\begin{aligned} & \text{minimize } F(\bar{x}) = (f_1(\bar{x}), f_2(\bar{x}), \dots, f_m(\bar{x})), \\ & \text{subject to } \bar{x} \in \Omega, \end{aligned} \quad (6)$$

where  $\Omega$  is decision space, and  $\bar{x}$  is a decision variable which defines a fragment-type RFID tag structure.

## 2.3. MOEA/D-GO for Fragmented Tag Design

To solve multi-objective problem defined as in (6), different multi-objective evolutionary algorithms (MOEAs) can be used. However, for fragmented tag of a large amount of fragment cells, an efficient MOEA algorithm is always desired.

Recently, a high-efficiency multiobjective optimization technique for fragmented antenna design, referred to as multiobjective evolutionary algorithm based on decomposition combined with enhanced genetic operators (MOEA/D-GO), was proposed [20]. MOEA/D-GO carries forward all advantages of MOEA/D and genetic algorithm (GA). Detailed introduction and flowchart of MOEA/D-GO can be found in [20].

For fragmented UHF tag design, MOEA/D-GO scheme must be combined with electromagnetic simulator. Typical block diagram in terms of HFSS as EM simulator is shown in Fig. 2. The optimization kernel is constructed by using MOEA/D and HFSS [24]. For function evaluation, Matlab [25] can be integrated into the optimizer. In our design in this paper, MOEA/D-GO is implemented by using Visual C++ 6.0. The overall computational cost is mainly determined by the EM simulator.

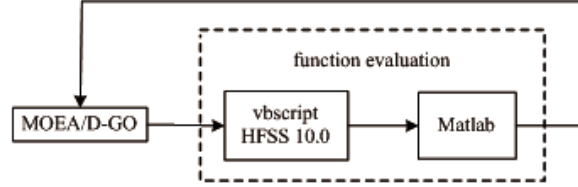


**Figure 2.** Block diagram of fragmented tag design with MOEA/D-GO.

### 3. FRAGMENTED TINY UHF RFID TAG DESIGN

For demonstration, we consider the design of a fragmented tiny square UHF tag operating at the 433 MHz, 869 MHz and 915 MHz RFID bands for an assumed chip impedance and the design of a fragmented round tiny RFID tag matching to several prevailing RFID chips at 915 MHz.

#### 3.1. Design of a Fragmented Multi-Band Square UHF Tag

The tiny fragmented square UHF tag is supposed to have dimensions of 5.5 mm \* 5.5 mm, which is approximately  $\lambda/60$  at 915 MHz. For fragmented structure design, the square tag area is gridded into cells of dimensions of 0.25 mm \* 0.25 mm (i.e., 22 \* 22 cells in total). The RFID chip is set at the center of the tag, where an area of 2 mm \* 1 mm (8 \* 4 cells) is left for the mount of a chip packaged with interposer.

Due to the broadband performance of fragmented antenna structure, we try a design by defining one objective instead of multiple objectives in (2), where a broad bandwidth covering the 433 MHz, 869 MHz and 915 MHz RFID bands is required. For example, we consider multi-band design for an assumed input impedance of  $10 - 64j$  ( $\Omega$ ). For this scenario, the MOEA/D-GO will reduce to ordinary single-objective genetic algorithm.

Several candidate fragmented tag structures have been obtained by running the optimization searching. Fig. 3 shows one of the fragment-type layouts.

Power transmission coefficient of fragmented tag with layout shown in Fig. 3 is calculated and depicted in Fig. 4. From the results presented in Fig. 4, we find that the optimized fragmented tiny UHF tag does have an operation bandwidth ranging from 320 MHz to 1020 MHz, if measured by power transmission coefficient of  $-0.46$  dB.

Therefore, tiny square UHF tag for RFID 433 MHz, 869 MHz and 915 MHz bands can be designed with fragment-type structure.

It should be remarked that presently available RFID chips for different RFID bands do not have the constant impedance as assumed in above design example. When designing tag versatile to different chip impedance at different RFID bands, multiple-objective combining (2) and (3) should be proposed.

#### 3.2. Design of a Versatile Fragmented Round UHF Tag

The tiny versatile fragmented round UHF tag is supposed to have diameter of 9 mm which is approximately  $\lambda/36$  at 915 MHz. For fragmented structure design, the round tag area is gridded into cells of dimensions of 0.5 mm \* 0.5 mm (i.e., 18 \* 18 cells in total). The RFID chip is to be set at the center of the tag, where an area of 1.2 mm \* 0.8 mm (3 \* 2 cells) is left for the mount of a packaged chip.

To demonstrate the versatility of fragment-type tag structure, we try to design a fragmented round tiny tag that can be connected to five commercial RFID chips at 915 MHz RFID band. Input impedances of five prevailing RFID chips at 915 MHz are listed in Table 1.

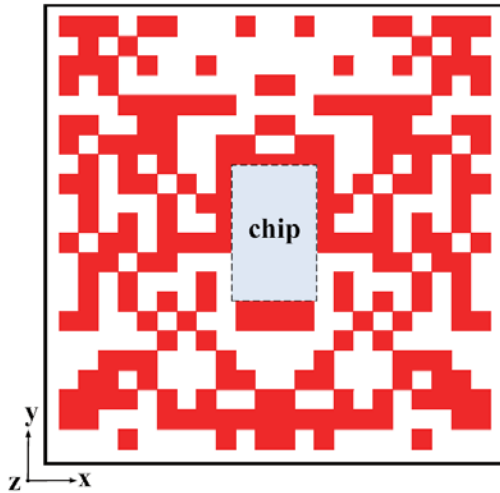


**Figure 3.** Layout of fragmented square tag for RFID 433 MHz, 869 MHz and 915 MHz bands.

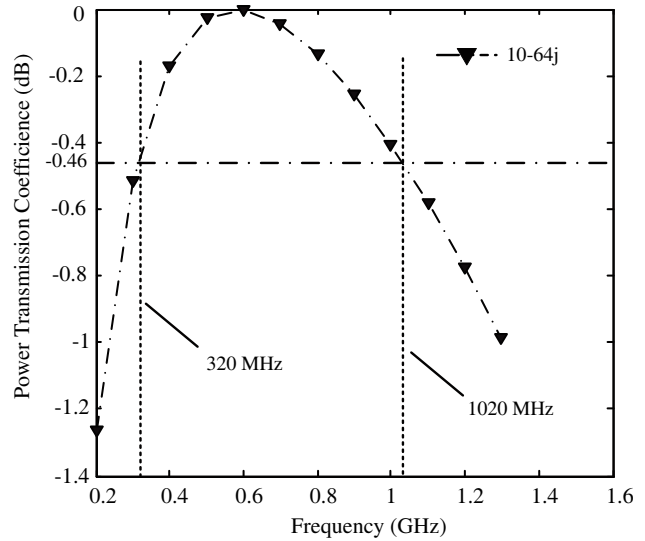


**Figure 4.** Power transmission coefficient of the tiny square tag connected to chip of input impedance of  $10 - 64j$  ( $\Omega$ ).

Two design schemes can be considered if a fragmented RFID tag is to be designed to fit all five chips. One is to define a power wave reflection coefficient for every of the five chips, which will yield five power wave reflection coefficients, and thus lead to a five-objective optimization problem as in (3). The other is to define two power wave reflection coefficients according to the upper and lower bounds of those chip impedances in Table 1, and to form a two-objective optimization problem as in (3).

**Table 1.** RFID chips for UHF RFID tags @ 915 MHz.

RFID chip	chip impedance $Z_{ci}$ ( $\Omega$ )	read sensitivity (dBm)
IMPINJ Monza-4 [26]	$11 - 143j$	-16.9
ALIEN Higgs-3 [27]	$27 - 195j$	-18
ALIEN Higgs-4 [28]	$18 - 181j$	-18.5
TI RI-UHF-STRAP-08 [29]	$10 - 64j$	-13
NXP UCODE G2XM [30]	$30 - 189j$	-15

It should be remarked that both the design schemes can be performed in another way by fixing the chip impedance, and varying the input impedance of tag antenna. This will lead to design of platform-tolerant tag. In general, input impedance of a designed tag antenna may change with the platform or object the tag attached. Defining a large dynamic range in the schemes will yield better tag tolerance.

Obviously, solving a two-objective optimization problem is easier than solving a five-objective optimization problem. From Table 1, we may define the two impedance bounds as  $Z_1 = 10 - 64j$  ( $\Omega$ ) and  $Z_2 = 30 - 195j$  ( $\Omega$ ). For  $Z_1$  and  $Z_2$ , two reflection coefficients ( $\Gamma_{p1}$  and  $\Gamma_{p2}$ ) can be defined according to (4), and thus the two design objectives can be specified as

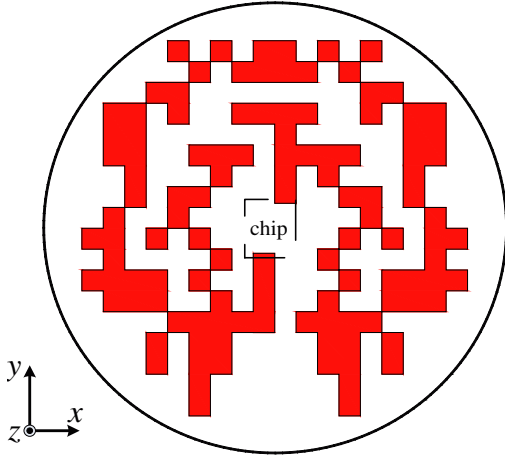
$$f_i(x) = \max(10 - |\Gamma_{pi}|_{\omega_i \in 915 \text{ MHz Band}}, 0) \quad (i = 1, 2), \quad (7)$$

As shown later in Section 4, design of fragmented RFID tag of versatile connection to any of the five prevailing UHF RFID chips can be attributed to a typical two-objective optimization problem as in (7).

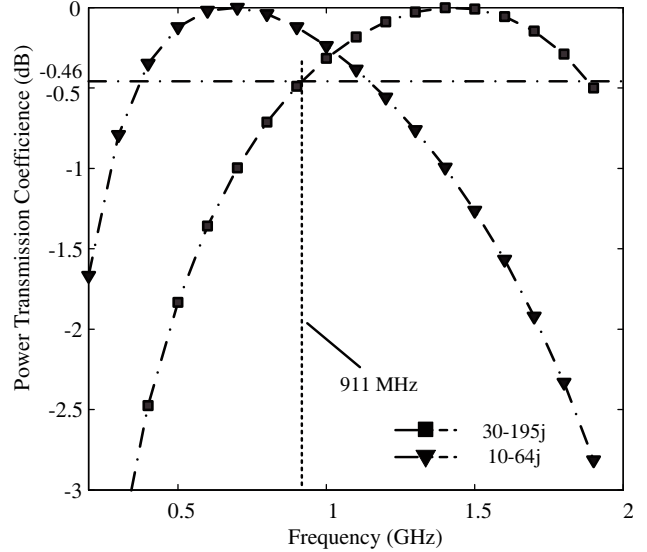
For the two-objective multi-objective problem, MOEA/D-GO optimization can be run to search optimal fragment distribution in the round area. Several candidate fragmented tag structures can be provided by the optimization searching.

Figure 5 shows one of the fragment-type tag layouts. Two power transmission coefficients of the fragmented tag are depicted in Fig. 6 when connected to “chip” of input impedance of  $Z_1 = 10 - 64j$  ( $\Omega$ ) and  $Z_2 = 30 - 195j$  ( $\Omega$ ), respectively.

From Fig. 6, we observe that the fragmented tag in Fig. 5 can operate for chips of input impedance of the upper and low bounds of impedances listed in Table 1. Therefore, it can be connected to any chips listed in Table 1. Detailed analysis of such versatility will be given in Section 4.



**Figure 5.** Layout of fragmented round tag for versatile connection to different RFID chips.



**Figure 6.** Power transmission coefficients of the versatile round tag when connected to chip of the upper and lower bound input impedance, respectively.

For verification, we connect IMPINJ Monza-4 ( $11 - 143j$ ) chip and ALIEN Higgs-3 ( $27 - 195j$ ) chip in Table 1 to the fragmented round tag structure, respectively. Prototypes of the designed fragmented tags on Rogers 4350b PCB, with two of them connected to IMPINJ Monza-4 and ALIEN Higgs-3 chip, are shown in Fig. 7. The Rogers 4350b PCB has a dielectric constant of 3.66, loss tangent of 0.004, and thickness of 1.524 mm.

Simulated power transmission coefficients for the tiny round tags connected to IMPINJ Monza-4 and ALIEN Higgs-3 chips are depicted in Fig. 8. Judging from the power transmission coefficients in Fig. 8, we find that the two chips can operate well on the fragmented round tag at 915 MHz RFID band. Fig. 9 shows the calculated non-normalized radiation pattern of antenna of the versatile fragmented round tag.

The two prototype RFID tags are tested by using Alien ALR-9900 RFID reader in a mono-static measurement. In the test, a linear polarized reader antenna with a gain of 6 dBi is used, and the reader system is set to have an EIRP of 1 W at 915 MHz. The test system is shown in Fig. 10.

Two basic fact will help the test scheme. First, the tiny round tag is so small that it will operate in the near field of the Alien reader antenna. Second, the tiny round tag has a dipole-like antenna pattern as shown in Fig. 9, thus we may have different read ranges when the tag is set at different orientations in front of the reader antenna.

When the round tag was set face-to-face with the reader antenna, we measured a maximum read range of approximately 22 cm for the tag with ALIEN Higgs-3 chip connected, and 19 cm for the tag with IMPINJ Monza-4 chip connected.

When the tag was set with its side to the reader antenna, we measured a maximum read range of approximately 30 cm for the tag with ALIEN Higgs-3 chip, and 25 cm for the tag with IMPINJ Monza-4 chip.

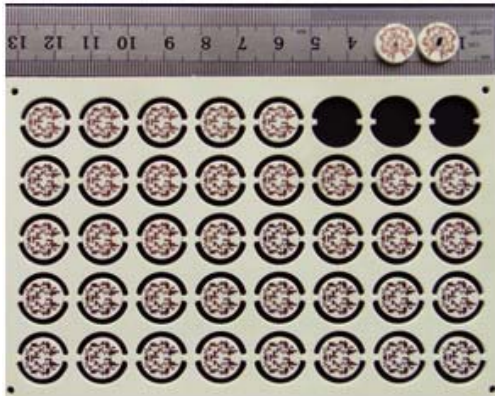


**Figure 7.** Prototypes of the fragmented versatile round tags, among which two are connected to IMPINJ Monza-4 chip (right) and ALIEN Higgs-3 chip (left).

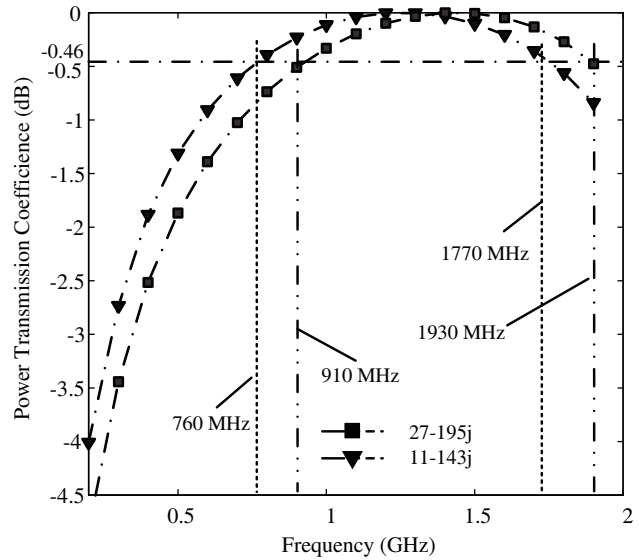


**Figure 8.** Power transmission coefficients of the versatile round tag with IMPINJ Monza-4 (11 – 143j) chip and ALIEN Higgs-3 (27 – 195j) chip, respectively.

With the read sensitivities of the two RFID chips listed in Table 1, we may evaluate the maximum read range. Comparison between the measured and evaluated maximum read ranges are listed in Table 2.

**Table 2.** Maximum read range for tags with different chips connected.

Tag	Tag-Reader deployment	measured (cm)	evaluated (cm)
IMPINJ Monza-4	face-to-face	19	25
	side-to-face	25	37
ALIEN Higgs-3	face-to-face	22	28
	side-to-face	30	43

Figure 11 depicts the measured read range patterns of the round tag with ALIEN Higgs-3 chip. The pattern has been normalized to the maximum read range. Since the tag is tested in near field, the read range pattern is somewhat different from the far-field radiation pattern shown in Fig. 9.

The round tags have also been tested when used for medical tube identification. In the test, we embedded a round tag into a plastic lid of medical tube (with blood filled up to 2/3, as shown in the enlarged picture in Fig. 10). The measured maximum read ranges are almost the same as reported above, which means the tiny round tag has a stable performance.

The reason that medical tube has little effects on the maximum read range can be shown in Fig. 12. Fig. 12 depicts the simulated power transmission coefficients of fragmented round tag of IMPINJ Monza-4 chip in case with and without a medical tube. Only minor effects of medical tube can be observed on its power transmission coefficient.

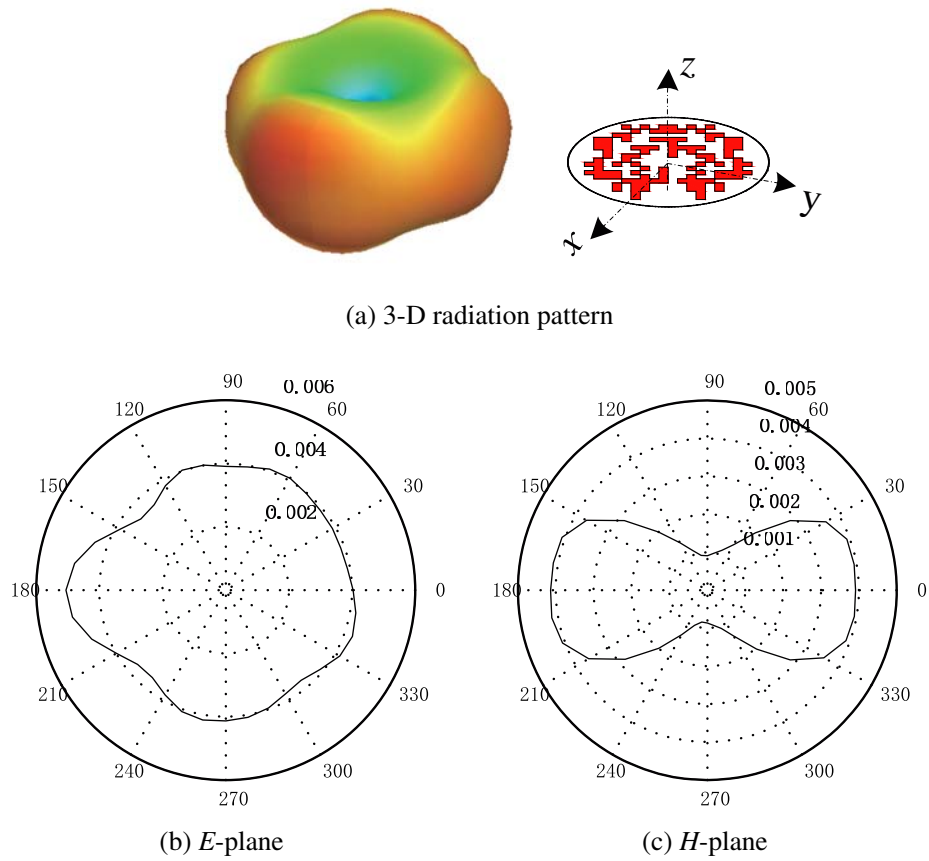


**Figure 9.** Radiation patterns of antenna of the tiny fragmented round tag.

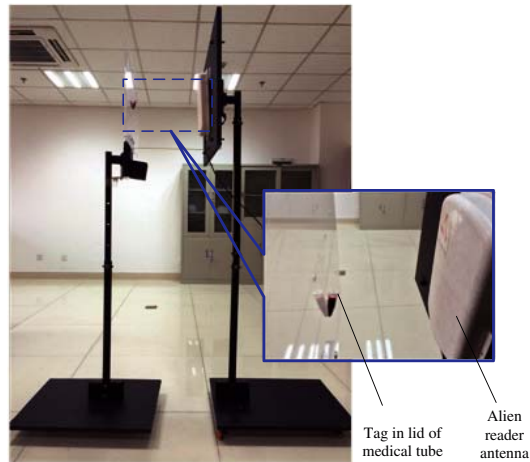


**Figure 10.** RFID test system with Alien-9900 RFID reader and antenna.

## 4. FURTHER DISCUSSION

### 4.1. Effects of Chip Impedance on Reflection Coefficient

In the design of versatile tiny round tag in Section 3, we defined two objectives in terms of the upper and low bound impedances, instead of using five objectives for chips listed in Table 1. Although both the simulations and tests with IMPINJ Monza-4 and ALIEN Higgs-3 chips demonstrate the feasibility

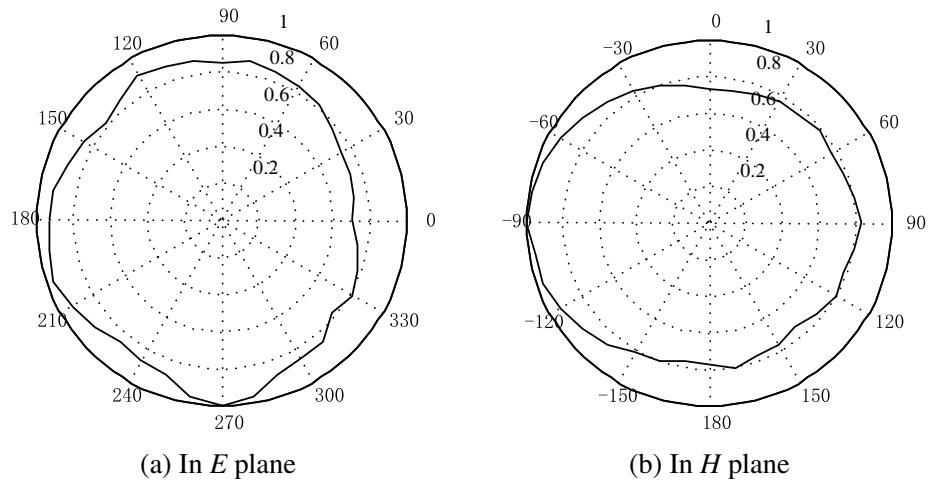


**Figure 11.** Normalized read range pattern of the round tag with ALIEN Higgs-3 chip.

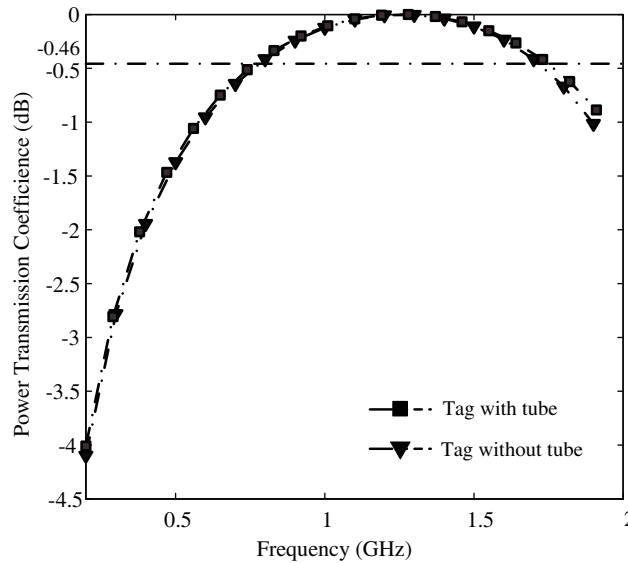


**Figure 12.** Comparison between the power transmission coefficients of tiny round tag with/without a medical tube.

of this design scheme, the underlying physics is still unclear why chips with impedances within the bounds operate quite well.

To give a better understanding of the power transmission coefficients shown in Fig. 6 and Fig. 8, we investigate the effects of resistance ( $R$ ) and reactance ( $X$ ) of RFID chip impedance on power wave reflection coefficient of the designed tag in Fig. 5.

By connecting the versatile round tag to chips of different impedances, Fig. 13 shows clearly the effects of chip resistance and reactance on the reflection coefficient. Fig. 13(a) and Fig. 13(b) depict reflection coefficient for chips with upper and lower resistance bound values in Table 1, but different reactance values. Fig. 13(c) and Fig. 13(d) depict reflection coefficient for chips with upper and lower reactance bound values in Table 1, but different resistance values.

From Fig. 13(a) and Fig. 13(b), we find that when connected to chips with larger reactance values, the versatile tag tends to shift its operation band to high frequency ends. From Fig. 13(c) and Fig. 13(d), we find that when connected to chips with larger resistance values, the versatile tag tends to reduce its operation bandwidth. That is why we observe in Fig. 6 that designated 915 MHz operation point is

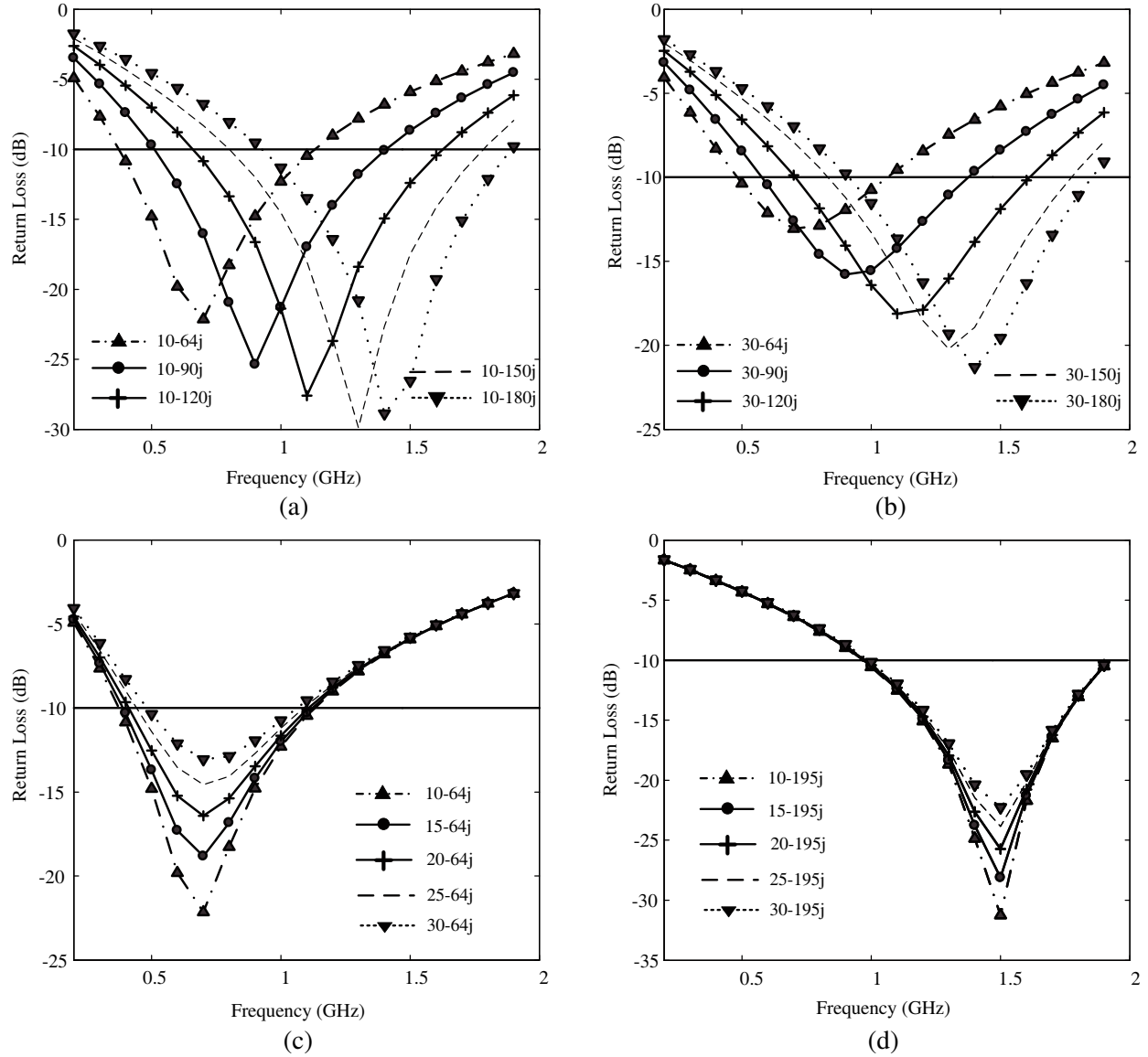


**Figure 13.** Effects of chip impedance on reflection coefficients.

located near the lower end of operation band for chip of impedance  $30 - 195j$  ( $\Omega$ ), while located near the upper end of operation band for chip of impedance of  $10 - 64j$  ( $\Omega$ ).

With the effects shown in Fig. 13, we may predict that if the versatile tag is connected to a chip listed in Table 1, the operation band will lay between the two regions characterized in Fig. 6. The operation bands shown in Fig. 8 are therefore a direct outgrowth.

#### 4.2. Effects of Adjunct Cells in the Fragmented Tag

The current distribution on the designed fragment-type tag is shown in Fig. 14. It is observed that some of the cells in the fragmented geometry form a loop for electric current. However, there are quite some cells being key adjunct to the current loop.

To show the effects of these adjunct cells, we may remove them and investigate the power transmission coefficients. Fig. 15 shows a simplified fragmented tag by keeping cells in the current loop. Fig. 16 shows the power transmission coefficients of the simplified tag when chips of resistance  $R = 11$  ( $\Omega$ ) and critical reactance values are connected for operation at 915 MHz.

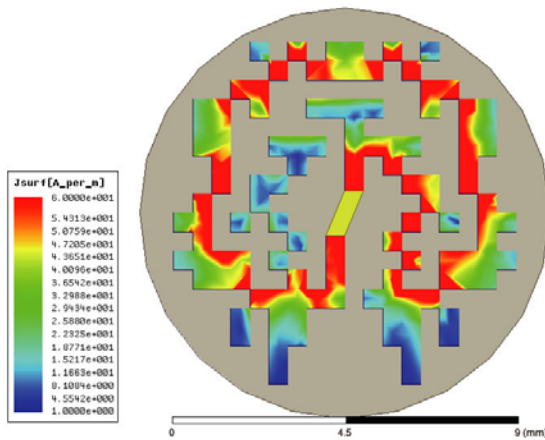


Figure 14. Current distribution on prototype of fragmented tag.

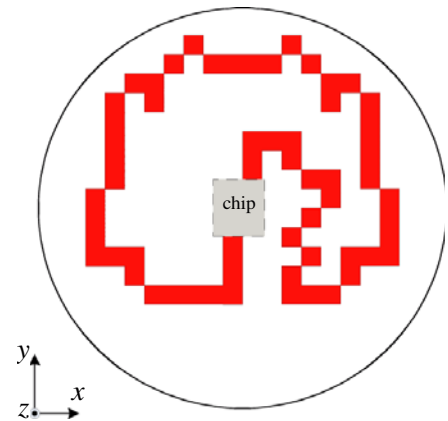


Figure 15. Simplified tag with cells in the current loop.

From Fig. 16, it is observed that the simplified loop allows a small dynamic range of input impedance of chip in order to guarantee its operation at 915 MHz. The impedance now ranges from  $11 - 60j \ (\Omega)$  to  $11 - 160j \ (\Omega)$ , while for original tag in Fig. 5 it ranges from  $11 - 50j \ (\Omega)$  to  $11 - 195j \ (\Omega)$ . Therefore, the adjunct cells do benefit the versatility of the fragmented tag.

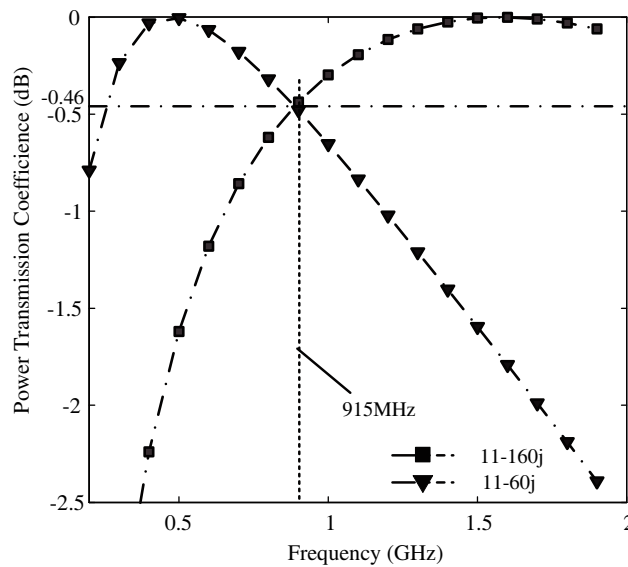


Figure 16. Power transmission coefficients of the simplified tag when connected to two critical bound impedances.

### 5. CONCLUSION

UHF RFID tags with fragment-type structure can be designed for multi-band operation and for versatile connection to different RFID chips, which may benefit the design and production of RFID tags.

By defining multiple objectives according to different design requirements, MOEA/D-GO can be used for optimization searching of fragment-type structure of tag. This technique shows the potential to be a universal design technique because there is no restriction on dimensions and shape of tag to be designed.

Tiny fragmented UHF RFID tags for medical tube has been designed and tested. The versatility of fragmented tiny tag is demonstrated. More tiny RFID tags for different industry products or components (including metalwork) can be designed in fragmented structures.

## ACKNOWLEDGMENT

This work was supported in part by the National Natural Science Foundation of China under Grant 61272471.

## REFERENCES

1. Deng, J. H., W. S. Chan, B. Z. Wang, S. Y. Zheng, and K. F. Man, "An RFID multicriteria coarse- and fine-space tag antenna design," *IEEE Trans. Ind. Electron.*, Vol. 58, 2522–2530, 2011.
2. Babar, A., A. Elsherbeni, L. Sydanheimo, and L. Ukkonen, "RFID tags for challenging environments: Flexible high-dielectric materials and ink-jet printing technology for compact platform tolerant RFID tags," *IEEE Microwave Mag.*, Vol. 14, 26–35, 2013.
3. Marrocco, G., "Pervasive electromagnetics: Sensing paradigms by passive RFID technology," *IEEE Wireless. Commun.*, Vol. 17, 10–17, 2010.
4. Gao, J., J. Siden, and H.-E. Nilsson, "Printed electromagnetic coupler with an embedded moisture sensor for ordinary passive RFID tags," *IEEE Electr. Devi. Lett.*, Vol. 32, 1767–1769, 2011.
5. Virtanen, J., L. Ukkonen, T. Bjorninen, A. Z. Elsherbeni, and L. Sydanheimo, "Inkjet-printed humidity sensor for passive UHF RFID systems," *IEEE Trans. Instrument. Measur.*, Vol. 60, 2768–2777, 2011.
6. Virkki, J., T. Bjorninen, T. Kellomaki, S. Merilampi, I. Shafiq, L. Ukkonen, L. Sydanheimo, and Y. C. Chan, "Reliability of washable wearable screen printed UHF RFID tags," *Microelectron. Reliab.*, Vol. 54, 840–846, 2014.
7. Amin, Y., Q. Chen, L. R. Zheng, and H. Tenhunen, "Development and analysis of flexible UHF antennas for green electronics," *Progress In Electromagnetics Research*, Vol. 130, 1–15, 2012.
8. Choo, H., A. Hutani, L. C. Trintinalia, and H. Ling, "Shape optimisation of broadband microstrip antennas using genetic algorithm," *Electr. Lett.*, Vol. 36, 2057–2058, Dec. 2000.
9. Herscovici, N., M. Osorio, and C. Peixeiro, "Miniaturization of rectangular microstrip patches using genetic algorithms," *IEEE Antennas Wirel. Propag. Lett.*, Vol. 1, 94–97, Jan. 2002.
10. Pringle, L. N., P. H. Harms, S. P. Blalock, G. N. Kiesel, E. J. Kuster, P. G. Friederich, R. J. Prodo, J. M. Morris, and G. S. Smith, "A reconfigurable aperture antenna based on switched links between electrically small metallic patches," *IEEE Trans. Antennas Propag.*, Vol. 52, 1434–1445, Jun. 2004.
11. Thors, B., H. Steyskal, and H. Holter, "Broad-band fragmented aperture phased array element design using genetic algorithms," *IEEE Trans. Antennas Propag.*, Vol. 53, 3280–3287, Oct. 2005.
12. Ethier, J., D. McNamara, M. Chaharmir, and J. Shaker, "Reflectarray design using similarity-shaped fragmented sub-wavelength elements," *Electr. Lett.*, Vol. 48, 900–902, 2012.
13. Soontornpipit, P., C. M. Furse, and Y. C. Chung, "Miniaturized biocompatible microstrip antenna using genetic algorithm," *IEEE Trans. Antennas Propag.*, Vol. 53, 1939–1945, Jun. 2005.
14. John, M. and M. Amman, "Wideband printed monopole design using a genetic algorithm," *IEEE Antennas Wirel Propag. Lett.*, Vol. 6, 447–449, 2007.
15. Kim, G. J. and Y. C. Chung, "Optimization of UHF RFID tag antennas using a genetic algorithm," *Proc. IEEE Int. Symp. Antennas Propag.*, 2087–2090, 2006.
16. Jin, Z., H. Yang, X. Tang, and J. Mao, "Impedance analysis of the fragment-type tag antenna using FDTD," *Proc. 8th Int. Symp. Antennas, Propag. and EM Theory*, 260–262, 2010.
17. Jin, Z., H. Yang, X. Tang, and J. Mao, "Parameters and schemes selection in the optimization of the fragment-type tag antenna," *Proc. 3rd Int. Joint Conf. Comput. Sci. Optim.*, Vol. 2, 259–262, 2010.

18. Zhang, Q. and H. Li, "MOEA/D: A multiobjective evolutionary algorithm based on decomposition," *IEEE Trans. Evol. Comput.*, Vol. 11, No. 6, 712–731, Dec. 2007.
19. Li, H. and Q. Zhang, "Multiobjective optimization problems with complicated pareto sets, MOEA/D and NSGA-II," *IEEE Trans. Evol. Comput.*, Vol. 13, 284–302, Apr. 2009.
20. Ding, D. and G. Wang, "MOEA/D-GO for fragmented antenna design," *Progress In Electromagnetics Research M*, Vol. 33, 1–15, 2013.
21. Marrocco, G., "The art of UHF RFID antenna design: Impedance-matching and size-reduction techniques," *IEEE Antennas Propag. Mag.*, Vol. 50, No. 1, 66–79, 2008.
22. Loo, C. H., K. Elmahgoub, and F. Yang, "Chip impedance matching for UHF RFID tag antenna design," *Progress In Electromagnetics Research*, Vol. 81, 359–370, 2008.
23. Kurokawa, K., "Power waves and the scattering matrix," *IEEE Trans. Microwave Theory and Techniques*, Vol. 13, 194–202, 1965.
24. Ansoft HFSS (High Frequency Structure Simulator), <http://www.ansoft.com/products/hf/hfss/>.
25. Matlab (Matrix Laboratory), <http://www.mathworks.cn/products/matlab/>.
26. Impinj Monza-4, [http://www.impinj.com/Monza\\_RFID\\_Chips.aspx](http://www.impinj.com/Monza_RFID_Chips.aspx).
27. Alien Higgs-3, <http://www.alientechnology.com/ic/>.
28. Alien Higgs-4, <http://www.alientechnology.com/ic/>.
29. TI RI-UHF-STRAP-08, <http://www.alldatasheet.com/datasheet-pdf/pdf/-177692/TI/RI-UHF-STRAP-08.html>.
30. NXP UCODE G2XM, [http://www.nxp.com/products/identification\\_and\\_security/smart\\_label\\_and\\_tag\\_ics/ucode/#overview](http://www.nxp.com/products/identification_and_security/smart_label_and_tag_ics/ucode/#overview).